Hindawi
Mathematical Problems in Engineering
Volume 2020, Article ID 1571439, 10 pages
https://doi.org/10.1155/2020/1571439

Research Article

Stable Balance Adjustment Structure of the Quadruped Robot Based on the Bionic Lateral Swing Posture

Jian-Hua Qin,[1] Jie Luo,[1] Kai-Chi Chuang,[1] Tian-Syung Lan,[2] Lie-Ping Zhang,[1] and Huai-An Yi[1]

[1]*College of Mechanical and Control Engineering, Guilin University of Technology, Guilin, Guangxi 541004, China*
[2]*Department of Information Management, Yu Da University, Miaoli County 36143, Taiwan*

Correspondence should be addressed to Tian-Syung Lan; tslan888@yahoo.com.tw

Received 21 June 2020; Revised 1 August 2020; Accepted 13 August 2020; Published 28 August 2020

Academic Editor: A. M. Bastos Pereira

Aiming at the problem that the stability of the quadruped robot is decreased as its leg momentum is too high, a stable balance adjustment structure of the quadruped robot based on the bionic lateral swing posture is proposed. First, the leg structure of the quadruped robot is improved and designed by using the mechanism of the lateral swing posture of the leg of the hoof animal. Then, the D-H method is used to construct the corresponding leg kinematics model and determine the generalized coordinates of the leg joints in the lateral swing posture. The torque expression of the quadruped robot when it is tilted is established. Based on the differential equation of momentum of the hip joint and its static stability analysis, the static stability conditions in the upright posture and the bionic lateral swing posture are given. Finally, the experimental simulation and comparative analysis of the upright posture and the lateral swing posture of the quadruped robot are proposed by using the Adams virtual prototype technology. The simulation results show that as the angle of lateral swing increases, the peak value of the positive flip torque of the quadruped robot body increases accordingly, while the degree of tilt decreases accordingly, which shows that the bionic lateral swing posture of the quadruped robot has higher static stability than the traditional upright posture. This research provides a technical reference for the design and optimization of the offline continuous gait of the robot and the improvement of stability.

1. Introduction

The quadruped robot has high nonlinear dynamic characteristics and can work in the unstructured environment, which is a hot research topic in the field of industrial robots. Good stability is the basis for the robot to perform real-time operations, and it is also a major and difficult point in the study of quadruped robots [1–3]. At present, scholars at home and abroad mostly adopt the design and optimization of the structure of the robot or improve the control algorithm to achieve the stability of the robot. Chen et al. proposed a new type of robot leg structure and control method, aiming at the problems of large inertia of legs and difficulty in control for quadruped robots [4]. The optimized segmented Hermite difference method was used to plan the foot trajectory of the quadruped robot, and a good control effect was obtained. Nemoto et al. have developed a reconfigurable quadruped robot that can perform walking and rolling movements [5]. The proposed energy-based controller can effectively achieve periodic motion on a plane. Gor et al. proposed a pair of orthogonally mounted moving appendages mechanism to accommodate locked joint failure and a three-dimensional multibody dynamics model of quadruped robot, and its fault accommodation strategies are developed and the control performance is validated both through simulations and experiments [6]. He et al. designed an adaptive neural network (NN) controller involving an integral barrier Lyapunov function (IBLF) to deal with the end effector motion tracking issues of the manipulator [7]. The learning method based on the radial basis function NN (RBFNN) was applied to the controller, which compensates for the dynamic uncertainty and ensures the stability and coordination of the control of the manipulator. He et al. developed a reinforcement learning (RL) control strategy

based on an actor-critic structure and discussed the convergence and stability of the RL controller, used Lyapunov's direct method, and proved that the closed-loop system with the proposed RL control algorithm is to be semiglobal uniform ultimate bounded (SGUUB) [8].The control approach presented was tested on the discretized ODE dynamic model, which provides an effective solution for the stable control of the system. Farid et al. used the D-H notation to establish a mathematical model to determine the center of gravity of the robot, a simulation model was created in the MATLAB, Simulink environment and the robot's characteristic posture were analysed, and the robot's static stability was achieved by properly aligning the feet [9]. Park et al. used a combined Jacobian of COG and centroid of a support polygon including a foot contact constraint to achieve a new trajectory planning algorithm , so that the robot was able to perform various modes of locomotion both in simulations and experiments with improved stability [10]. The abovementioned studies have achieved important results and provided valuable experience for the stability study of robots, but neglected the influence of robot leg momentum on robot stability in the presence of inertia. In response to this problem, a stabilization and balance adjustment structure of a quadruped robot based on a bionic lateral swing posture was proposed in this paper, and the design of the leg structure of the quadruped robot was improved. The corresponding leg kinematics model was constructed, the relationship between the foot position and the joint angle was determined, and the torque expression when the quadruped robot was tilted was established. The corresponding leg kinematics model was constructed, the relationship between the foot position and the joint angle was determined, and the torque expression when the quadruped robot was tilted was established. The static stability analysis was carried out and the static stability conditions of the quadruped robot with the traditional upright posture and bionic lateral swing posture were given, and the simulation experiments and comparative analysis of the upright posture and the lateral swing posture of the robot were carried out.

2. Improved Design of the Bionic Lateral Swing Structure of the Leg of the Quadruped Robot

2.1. Mechanism of the Bionic Lateral Swing Posture of the Leg. When animals perform certain special actions, they will change the support structure according to the mass distribution of each part to maintain the stability of the body. The ability of this posture to change with the external environment can help animals to improve their adaptability and survival ability to nature.

The giraffe's posture when drinking water is shown in Figure 1. In the figure, the point P is the projection of the center of mass of the giraffe on the ground, the quadrilateral EFGH is the support area in the upright posture, and EF is the short side of the quadrilateral. When in the stooped drinking posture, the leg swings outward at an angle θ, the area of the support area increases to a quadrilateral E′F′G′H′, the short side EF changes to the long side E′F′, and the shortest distance of the point P to the support boundary increases from d to d′. Therefore, this posture can shorten the distance between the head and the water surface, while increasing the support area and maintaining the balance of the body. This lateral swing posture can be used to improve the static stability for a quadruped walking robot whose structural parameters such as mass, leg length, and joint rotation angle are quantitative.

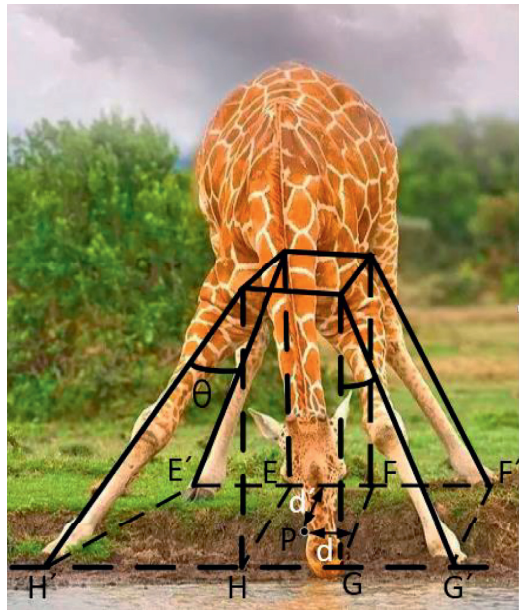

Figure 1: The swinging support of the giraffe's legs.

2.2. Improved Design of the Leg Structure. According to the abovementioned leg posture mechanism, this paper designs a small series quadruped robot with a motor as the driving element. The 3D model of the leg is shown in Figure 2. There are three degrees of freedom per leg of the robot, which are the side swing of the hip joint, the pitch of the hip joint, and the pitch of the knee joint. The joints are driven by worms that have the characteristics of reverse self-locking, so that the body can withstand a corresponding degree of lateral torque when it is in a lateral swing posture. The thigh adopts a splint design and the calf adopts a sleeve design and is provided with a damping, spring, and a rubber foot end to reduce the rigid impact caused by the outside during the movement of the robot. In order to ensure that the robot can reach a larger working space and improve the flexibility of the robot, the thigh and the calf are designed to have the same length [11]. The 3D model of the robot is shown in Figure 3.

3. Determination of the Robot Kinematics Model and Static Stability Conditions

3.1. Kinematics Model of the Leg. Robot kinematics describes the relationship between the joint angle and end posture during movement [12]. The right front leg was taken as an example in this article, and the kinematics model of the

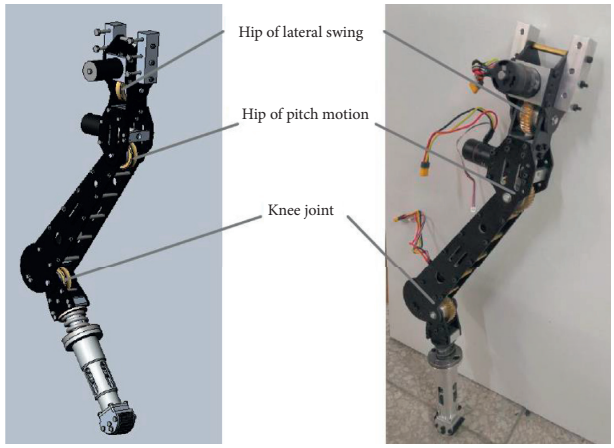

Figure 2: The leg structure of the robot.

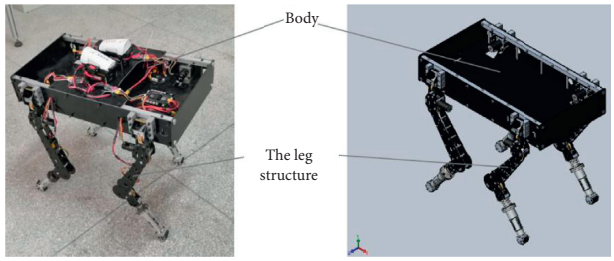

Figure 3: 3D model of the quadruped robot.

robot was established by using the D-H method. The joint coordinate system of the right front leg is shown in Figure 4, where O-XYZ is the global coordinate system and O_b-$X_bY_bZ_b$ is the reference coordinate system (also known as the body coordinate system).

To solve the position and pose of the foot end, it is necessary to perform the D-H transformation on the homogeneous transformation matrix corresponding to each joint in order to establish the kinematics equation of the robot [13]. According to the representation of each coordinate system in Figure 4 and the coordinate transformation rules of the D-H method, the coordinate transformation matrix of each joint of the right front leg can be obtained as follows:

$$T_b^0 = \begin{bmatrix} 0 & 0 & 1 & X_0 \\ -1 & 0 & 0 & Y_0 \\ 0 & -1 & 0 & Z_0 \\ 0 & 0 & 0 & 1 \end{bmatrix}, \tag{1}$$

$$T_0^1 = \begin{bmatrix} \cos\theta_1 & 0 & \sin\theta_1 & l_1\cos\theta_1 \\ \sin\theta_1 & 0 & -\cos\theta_1 & l_1\sin\theta_1 \\ 0 & 1 & 0 & 0 \\ 0 & 0 & 0 & 1 \end{bmatrix}, \tag{2}$$

$$T_1^2 = \begin{bmatrix} \cos\theta_2 & -\sin\theta_2 & 0 & l_2\cos\theta_2 \\ \sin\theta_2 & \cos\theta_2 & 0 & l_2\cos\theta_2 \\ 0 & 0 & 1 & 0 \\ 0 & 0 & 0 & 1 \end{bmatrix}, \tag{3}$$

$$T_2^3 = \begin{bmatrix} \cos\theta_3 & -\sin\theta_3 & 0 & l_3\cos\theta_3 \\ \sin\theta_3 & \cos\theta_3 & 0 & l_3\cos\theta_3 \\ 0 & 0 & 1 & 0 \\ 0 & 0 & 0 & 1 \end{bmatrix}. \tag{4}$$

In equation (1)–(4), X_0, Y_0, and Z_0 are the coordinates of the origin O_0 of the lateral swing hip coordinate system in the body coordinate system, and l_1, l_2, and l_3 are the lengths of the hip, thigh, and calf, respectively. The transformation matrix that can represent the foot end of the body coordinate system can be obtained as follows:

$$T_b^3 = \begin{bmatrix} R_3 & P_3 \\ O & I \end{bmatrix} = T_b^0 T_0^1 T_1^2 T_2^3 = \begin{bmatrix} s_{(2+3)} & c_{(2+3)} & 0 & l_2 s_2 + l_3 s_{(2+3)} + X_0 \\ -c_1 c_{(2+3)} & c_1 s_{(2+3)} & -s_1 & -l_1 c_1 - l_2 c_1 c_2 - l_3 c_1 c_{(2+3)} + Y_0 \\ -s_1 c_{(2+3)} & s_1 s_{(2+3)} & c_1 & -l_1 s_1 - l_2 s_1 c_2 - l_3 s_1 c_{(2+3)} + Z_0 \\ 0 & 0 & 0 & 1 \end{bmatrix}. \tag{5}$$

In equation (5), $s_1 = \sin\theta_1$, $c_1 = \cos\theta_1$, $s_{(2+3)} = \sin(\theta_2 + \theta_3)$, and $c_{(2+3)} = \cos(\theta_2 + \theta_3)$.

The coordinates of the foot end relative to the body coordinate system are as follows:

$$P_3 = \begin{bmatrix} P_x \\ P_y \\ P_z \end{bmatrix} = \begin{bmatrix} l_2\sin\theta_2 + l_3\sin(\theta_2+\theta_3) + X_0 \\ -l_1\cos\theta_1 - l_2\cos\theta_1\cos\theta_2 - l_3\cos\theta_1\cos(\theta_2+\theta_3) + Y_0 \\ -l_1\sin\theta_1 - l_2\sin\theta_1\cos\theta_2 - l_3\sin\theta_1\cos(\theta_2+\theta_3) + Z_0 \end{bmatrix}. \tag{6}$$

The coordinates of the foot end relative to the lateral swing hip joint are:

$$\begin{bmatrix} P_x' P_y' P_z' \end{bmatrix} = \begin{bmatrix} l_2\sin\theta_2 + l_3\sin(\theta_2+\theta_3) \\ -l_1\cos\theta_1 - l_2\cos\theta_1\cos\theta_2 - l_3\cos\theta_1\cos(\theta_2+\theta_3) \\ -l_1\sin\theta_1 - l_2\sin\theta_1\cos\theta_2 - l_3\sin\theta_1\cos(\theta_2+\theta_3) \end{bmatrix}. \tag{7}$$

Combined with the inverse kinematics solution of the obtained foot-end coordinates, the rotation angle expression of each joint can be obtained as follows:

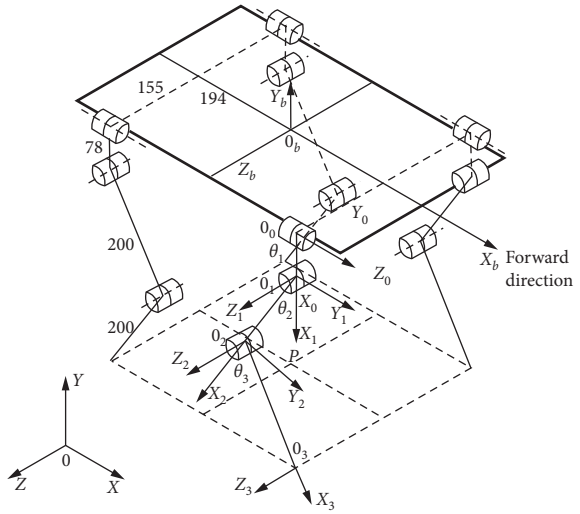

Figure 4: Sketch of the quadruped robot mechanism.

$$\begin{cases} \theta_1 = \tan^{-1}\left(\dfrac{p_y'}{p_z'}\right), \\ \theta_2 = \sin^{-1}\left(\dfrac{B_2}{\sqrt{P_x'^2 + B_1^2}}\right) - \cos^{-1}\left(\dfrac{P_x'}{\sqrt{P_x'^2 + B_1^2}}\right), \\ \theta_3 = \sin^{-1}\left(\dfrac{P_x' - l_2 \sin\theta_2}{l_3}\right) - \theta_2. \end{cases} \tag{8}$$

In equation (8),

$$\begin{cases} B_1 = \sqrt{P_x'^2 + P_y'^2} - l_1, \\ B_2 = \dfrac{l_3^2 - P_x'^2 - B_1^2 - l_2^2}{2l_2}. \end{cases} \tag{9}$$

It can be seen from equations (6) to (7) that, in the leg kinematics model of the robot, the joint rotation angle θ_i ($i = 1, 2, 3$) is used as the generalized coordinates to express the foot position and posture. When the vertical height of the fuselage is constant, θ_1 determines the lateral span of the robot, and θ_2 and θ_3 determine the distance that the robot can reach in the forward direction. When the robot walks straight, θ_1 does not change during the movement. When the robot is in an upright posture, θ_1 is always equal to 0°. When the robot is in a bionic lateral swing posture, θ_1 is rotated through a corresponding angle [14, 15].

3.2. Stability Conditions of the Body with a Traditional Upright Posture. Take the lifted state of the left hind leg as an example to determine the conditions of the static stability of the body [16]. Figure 5 shows the momentum, moment of the hip joint, and the leaning tendency of the body after the left hind leg is raised.

We consider the connecting rod between the joints of one leg as a mass point, so that one leg can be regarded as a mass point system. The first derivative of the moment of momentum ($\sum_{(i=1)}^{n} r_i \times m_i v_i$) applied by each mass point of a single leg to a fixed axis is equal to the algebraic sum of the moments (M_x) applied to the same axis by all forces (F_i) acting on these mass points [17, 18]. When the robot walks straight, the lateral swing hip joint of the leg does not participate in the movement, and the momentum and moment of the left hind leg hip joint can be expressed as follows:

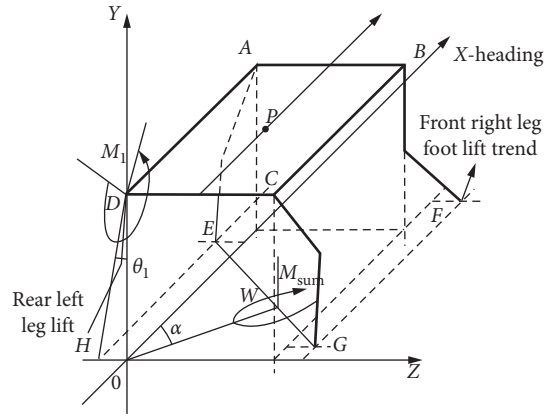

Figure 5: Schematic diagram of the movement state of the body when the left hind leg is lifted.

$$L_1 = \sum_{i=2}^{3} r_i \times m_i v_i. \tag{10}$$

According to the momentum theorem, the torque of the hip joint of the left rear leg can be written as

$$M_1 = \frac{dL_1}{dt} = \sum_{i=2}^{3} M_1\left(F_i^{(e)}\right). \tag{11}$$

It can be seen from Figure 5 that when the left rear leg is lifted, the tilt of the body changes through the turning axis passing through the E and G points. The torque received by the hip joint of the swing phase is added to the axis EG, which is assumed to be M_{sw}. In the traditional upright posture, M_{sw} can be expressed as follows:

$$M_{sw} = M_1 \cos\alpha = \left[M_1\left(F_i^{(e)}\right)\right]\cos\alpha. \tag{12}$$

In equation (12), α is the angle between the vertical component of the rotation plane where the moment of the hip joint in the swing phase lies and the rotation plane where M_{sw} lies.

As shown in Figure 6, the body support area during the left rear leg lift is ΔEFG. It can be deduced from the mathematical relationship:

$$\begin{cases} |OP| = |P_x|_E, \\ |OE| = \dfrac{b}{2} = |P_Z|_E, \\ |PE| = \sqrt{|OE|^2 + |OP|^2} = \sqrt{|P_Z|_E^2 + |P_x|_E^2}, \end{cases} \tag{13}$$

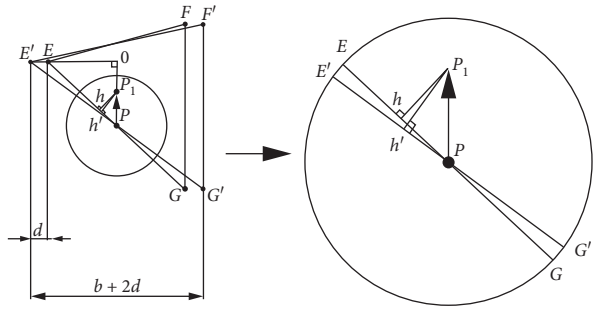

Figure 6: Schematic diagram of stability margin increment.

In the equation, $|P_x|_E$ and $|P_Z|_E$ are the X-coordinate of the foot E in the body coordinate system and the Z-coordinate of the foot E in the body coordinate system that determined by the initial value of θi ($i = 2, 3$) that characterizes the foot position of the robot. When the body advances a distance ds, the center of gravity P changes to P_1. Assuming that the X-coordinate of the foot end E in the body coordinates system is expressed as $|P_x|_{E1}$,

$$\mathrm{d}s = \mathrm{d}\left|PP_1\right| = \mathrm{d}\left|\left|P_x\right|_E - \left|P_x\right|_{E1}\right| = v_b \mathrm{d}t. \tag{14}$$

In equation (14), v_b is the speed of the fuselage relative to the ground in the forward direction. The measurement of the stability margin of the robot after the leg is lifted for t time is

$$\begin{aligned}\left|P_1 h\right| &= \frac{\left|PP_1\right| \times |OE|}{|PE|} = \frac{\int_0^t v_b \mathrm{d}t \times \left|P_Z\right|_E}{\sqrt{\left|P_Z\right|_E^2 + \left|P_x\right|_E^2}} \\ &= \frac{\int_0^t v_b \mathrm{d}t \times \left|Z_0\right|}{\sqrt{Z_0^2 + \left[l_2 s_2 + l_3 s_{(2+3)} + X_0\right]^2}}.\end{aligned} \tag{15}$$

In the traditional upright posture, the forward turning torque that the body acts on the axis EG can be expressed as

$$M_m = mg\left|P_1 h\right|. \tag{16}$$

In equation (16), m is the mass of the body. During the movement of the quadruped robot, at least one leg is required to swing to achieve the advancement of the body, and at the same time, the contact between the three legs and the ground is required to maintain static stability. The body must be restored to its equilibrium state before the swing phase becomes the support phase to achieve continuous offline walking of the body, so that the condition must be met after T/8 is as follows:

$$M_{sw} < M_m \longrightarrow \left[\sum_{i=2}^{3} M_1\left(F_i^{(e)}\right)\right]\cos\alpha < \frac{mg \times \int_0^{T/8} v_b \mathrm{d}t \times \left|Z_0\right|}{\sqrt{Z_0^2 + \left[l_2 s_2 + l_3 s_{(2+3)} + X_0\right]^2}}. \tag{17}$$

3.3. Stability Conditions of the Body with a Bionic Lateral Swing Posture. When the leg swings at an angle, the reverse torque M_{sw} of the leg of swing phase acts to the flip axis can be expressed as

$$M_{sw} = M_1 \cos\alpha \cos\theta_1 = \left[M_1\left(F_i^{(e)}\right)\right]\cos\alpha \cos\theta_1. \tag{18}$$

In equation (18), θ_1 is the angle at which the leg swings outward. The support area is $\triangle E'F'G'$. It can be derived from the mathematical relationship:

$$\begin{cases} \left|OE'\right| = \dfrac{b}{2} + d = \left|P_Z\right|_{E'}, \\ \left|PE'\right| = \sqrt{\left|OE'\right|^2 + |OP|^2} = \sqrt{\left|P_Z\right|_E^2 + \left|P_x\right|_E^2}, \end{cases} \tag{19}$$

where $|P_Z|_{E'}$ is the Z-coordinate of the foot end E' in the body coordinate system, which is determined by the initial value of θ_i ($i = 1, 2, 3$). The measurement of the stability margin of the robot after the leg is lifted for t time is shown as follows:

$$\begin{aligned}\left|P_1 h'\right| &= \frac{\left|PP_1\right| \times \left|OE'\right|}{\left|PE'\right|} = \frac{\int_0^t v_b \mathrm{d}t \times \left|P_Z\right|_{E'}}{\sqrt{\left|P_Z\right|_{E'}^2 + \left|P_x\right|_{E'}^2}} \\ &= \frac{\int_0^t v_b \mathrm{d}t \times \left[-l_1 s_1 - l_2 s_1 c_2 - l_3 s_1 c_{(2+3)} + Z_0\right]}{\sqrt{\left[-l_1 s_1 - l_2 s_1 c_2 - l_3 s_1 c_{(2+3)} + Z_0\right]^2 + \left[l_2 s_2 + l_3 s_{(2+3)} + X_0\right]^2}}.\end{aligned} \tag{20}$$

It can be seen from equations (19) and (20) that increasing the angle of the leg swinging laterally increases the lateral distance of the foot ends. Assuming that the lateral distance of the foot end can increase infinitely with the lateral swing angle, the distance travelled by the center of mass will be approximately equal to the stability margin measurement. In order to avoid the damage of the parts caused by excessive lateral moments of the hip joint in the lateral swing posture, the swing angle limit of θ_1 is set to $\theta_1 \in [-20^\circ, 20^\circ]$.

In the bionic lateral swing posture, the forward turning torque that the body acts on the axis EG can be expressed as

$$M_m = m_b g\left|P_1 h'\right|. \tag{21}$$

Equations (18) and (21) show that the lateral swing posture can not only reduce the reverse flip torque to the tilt axis generated by the swing phase but also increase the increments of the stability margin with time, so that the fuselage's balance can be restored quickly after tilting. The static stability conditions of the body are followed:

$$\begin{aligned}M_{sw} < M_m \longrightarrow &\left[\sum_{i=2}^{3} M_i\left(F_i^{(e)}\right)\right]\cos\alpha \cos\theta_1 \\ &< \frac{mg \times \int_0^{T/8} v_b \mathrm{d}t \times \left[-l_1 s_1 - l_2 s_1 c_2 - l_3 s_1 c_{(2+3)} + Z_0\right]}{\sqrt{\left[-l_1 s_1 - l_2 s_1 c_2 - l_3 s_1 c_{(2+3)} + Z_0\right]^2 + \left[l_2 s_2 + l_3 s_{(2+3)} + X_0\right]^2}}.\end{aligned} \tag{22}$$

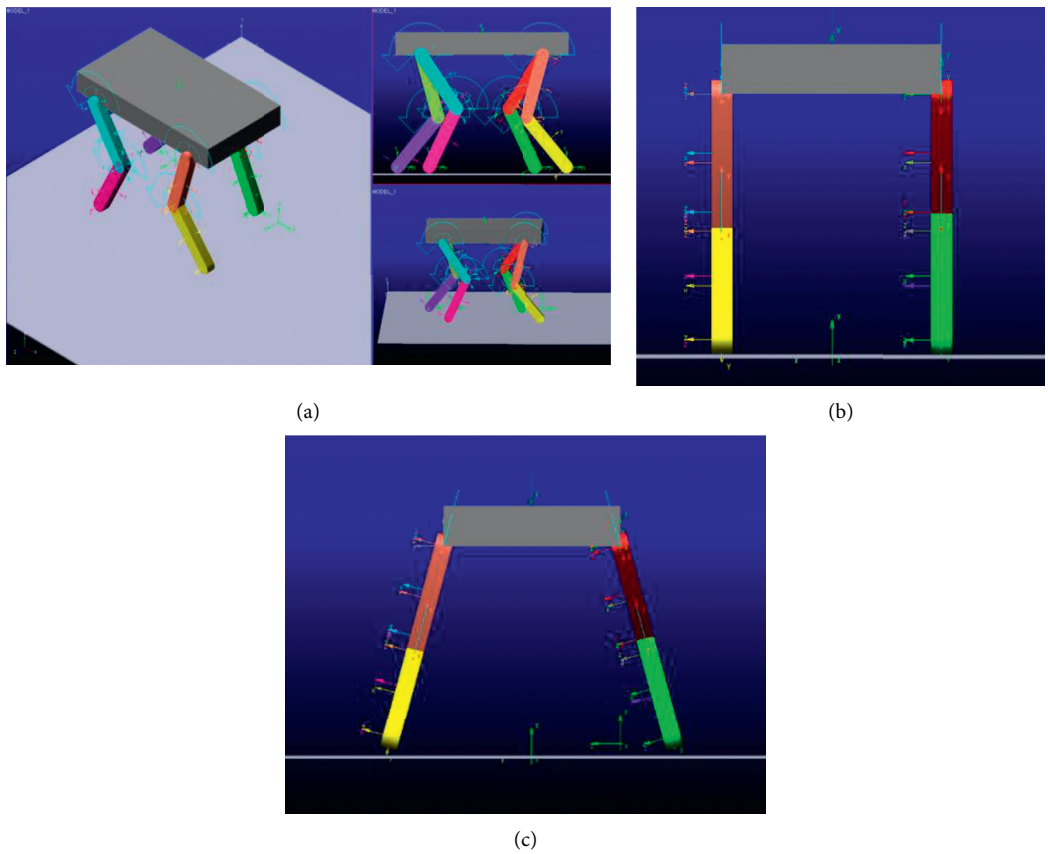

(a) (b)

(c)

Figure 7: The model of motion simulation. (a) Space view; (b) upright posture; and (c) lateral swing posture.

4. Experimental Simulation

4.1. Determination of the Simulation Scheme for Walking Experiment. To verify the static stability conditions of the quadruped robot walking offline continuously in different postures and the static stability advantages of the bionic lateral swing posture compared to the traditional upright posture, it is necessary to determine the load and the degree of tilt of the body. The solver of the automatic analysis software for mechanical system dynamics (ADAMS) adopts the Lagrangian equation method to establish system dynamics equations, which can perform statics, kinematics, and dynamics analysis on the virtual mechanical system, thereby obtaining time-varying curves about displacement, speed, acceleration, force, and torque. Through the output curve, the motion state of the system can be solved and analysed. The ADAMS is used to simulate the motion of the quadruped robot based on the traditional upright posture and the bionic lateral swing posture under the condition of duty cycle $\beta = 0.75$ in this paper. The step function and the mod function are jointly used to change the design of the driving joint angle of each leg of the robot with time, and the stepping order of the robot was set as follows: left rear leg-left front leg-right rear leg-right front leg. After the experimental simulation, the results are imported into a MATLAB drawing for comparative analysis. The motion simulation model is shown in Figure 7, where (a) is the model in the space view and (b) and (c) are the upright posture and the bionic lateral swing posture of the model, respectively. The main parameters of the designed gait are shown in Table 1.

4.2. Results and Discussion. In order to explore the change of the forward torque of the body with the lateral swing posture of the leg, the curve of the forward torque of the body's center of mass acting on the flip axis is as shown in Figure 8 after the walking motion simulation about the upright posture and the bionic lateral posture.

It can be seen from Figure 8 that the moment that the body acts on the tilt axis increases from the time when the rear leg is lifted to fall. The incremental change of torque with time is approximately the same during the process of raising the hind legs and falling off the front legs in each posture and increases with the increase of the lateral swing angle during the process of raising the front legs and the feeling of the hind legs. This shows that the lateral swing posture has a greater tendency to return to equilibrium after the body is tilted compared to the upright posture. The change of the torque curve at the peak position is not smooth due to the structural size error of the mechanical system.

The positive torque curve and the reverse torque curve of the turning axis of the quadruped robot within 0~T/8 are shown in Figure 9.

In Figure 9, due to the poor modeling environment of the quadruped robot mechanism in Adams, in the motion simulation results, the torque curve is not smooth, and there

Table 1: Main parameters of walk gait.

Leg posture	Gait cycle (T/s)	Step size (s/mm)	Distance of single leg step (mm)	Phase difference (φi)	Height of the body (H/mm)	Height of leg lift (mm)	Distance of feet on the same side (mm)
Upright posture	4	200	50	0.25	424	100	438
Lateral swing posture	4	200	50	0.25	424*cos θ_1	100*cos θ_1	438

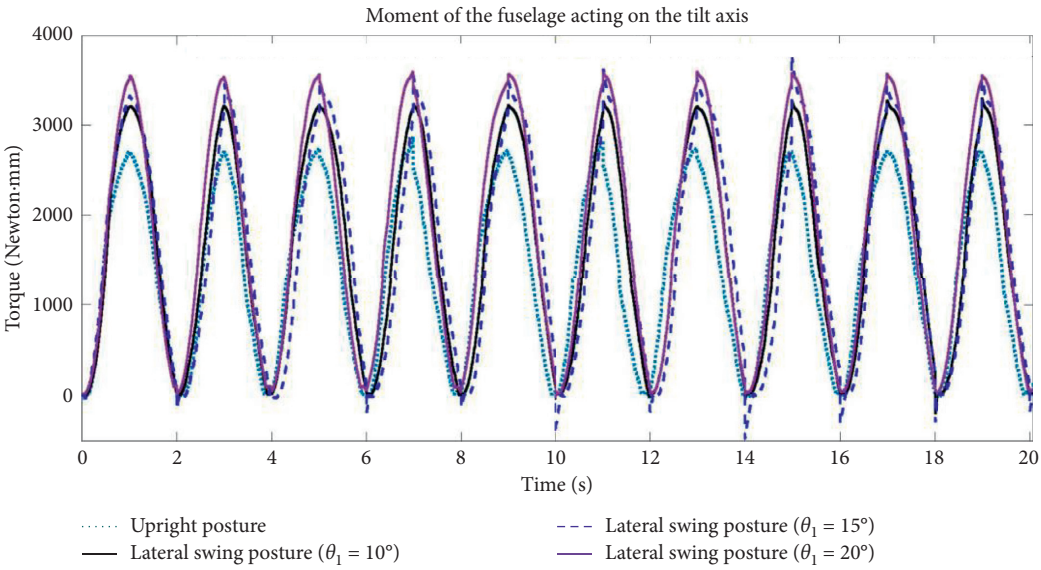

Figure 8: Moment of the fuselage acting on the tilt axis.

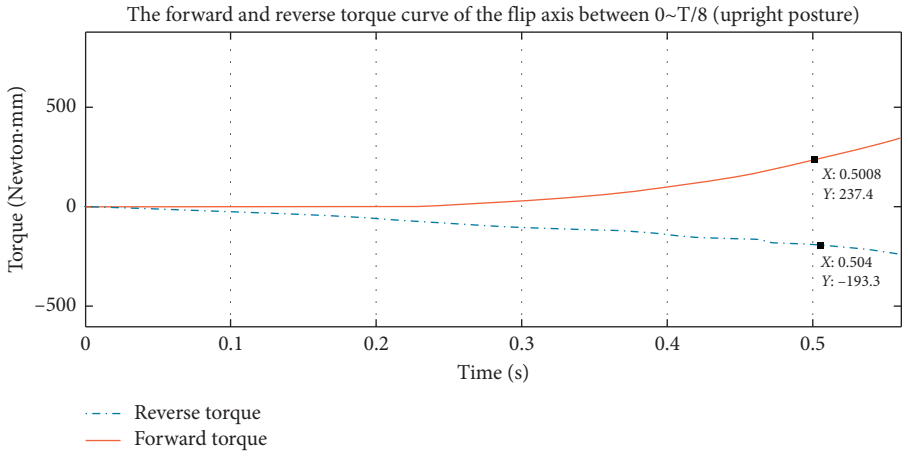

(a)

Figure 9: Continued.

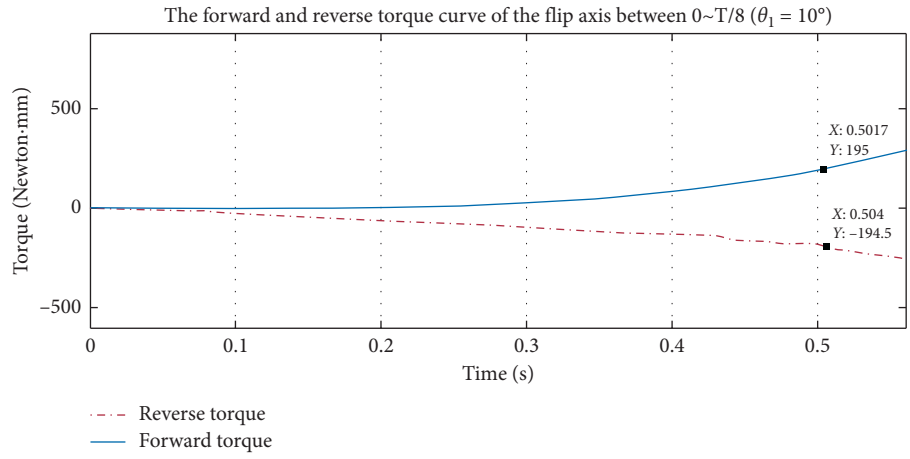

(b)

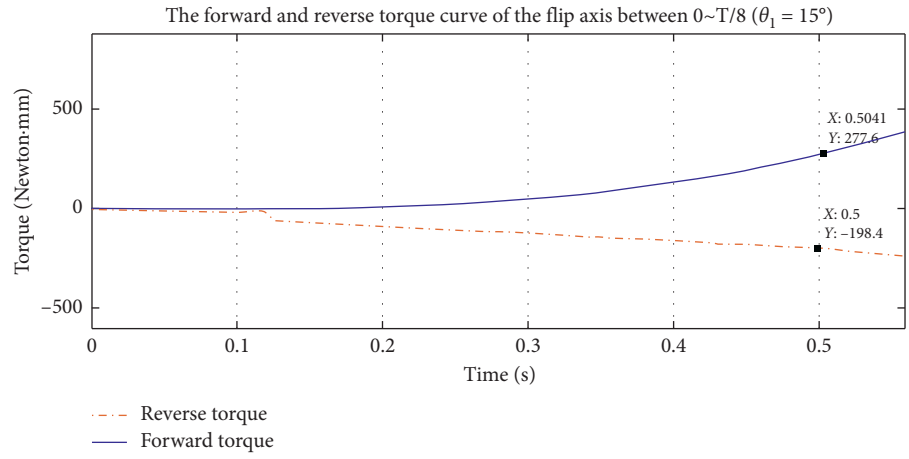

(c)

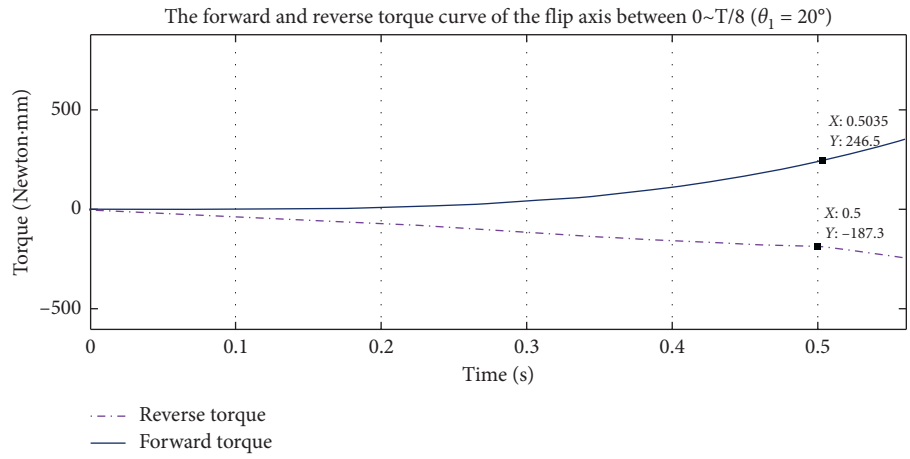

(d)

FIGURE 9: The forward and reverse torque curve of the flip axis between 0~T/8. (a) $\theta_1 = 0^\circ$. (b) $\theta_1 = 10^\circ$. (c) $\theta_1 = 15^\circ$. (d) $\theta_1 = 20^\circ$.

is a short-term longitudinal jitter in the reverse torque curve in (c). However, the change trend of the torque is not affected.

According to Figure 9(a)–9(c) and 9(d), the forward torque is greater than the reverse torque after T/8, indicating that, in these poses, the robot can meet the balance conditions and achieve offline continuous walking. By comparison, the difference of forward and reverse moments in the lateral swing posture of $\theta_1 = 10^\circ$ is smaller than that in the original upright attitude, so the stability effect of the lateral swing posture is not obvious. The difference in forward and reverse moments in the lateral swing posture of

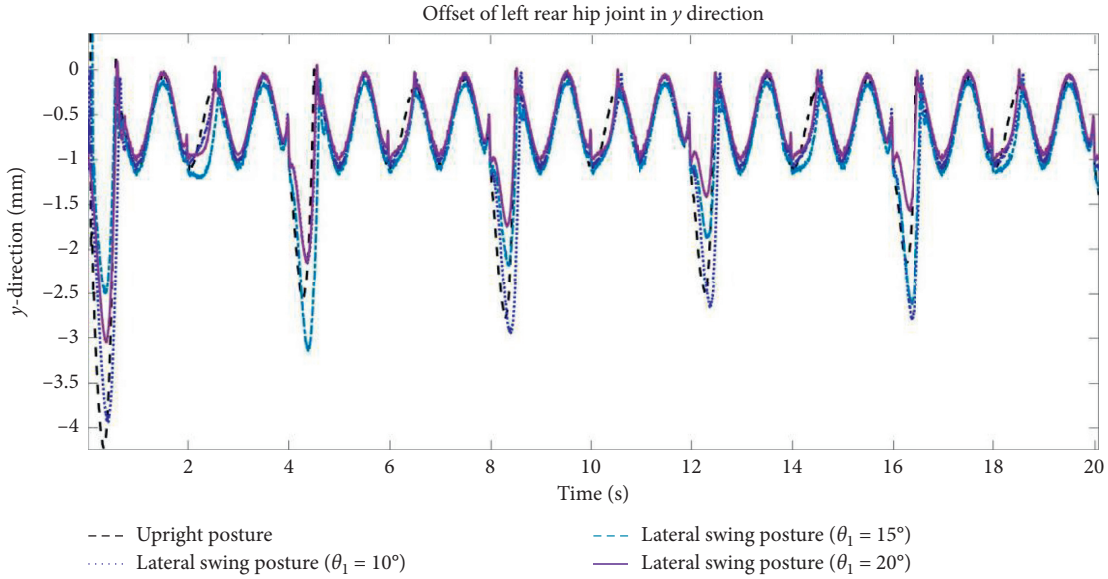

Figure 10: *Y*-direction fluctuation curve of the left posterior hip joint when walking straight.

$\theta_1 = 15^\circ$ and $\theta_1 = 20^\circ$ is greater than that in the original upright attitude, so the stability is improved relative to the original upright attitude.

In order to determine the degree of tilt of the robot during movement, the resulting y-direction fluctuation curve of the left rear hip joint is shown in Figure 10.

According to Figure 10, the maximum deviation of the left rear joint in the y-direction of each cycle occurs when the left rear leg is raised to the highest position, the maximum offset distance in the whole walking process occurs in the first step of the first cycle, and the maximum offset distance decreases with the increase of the lateral swing angle. According to the y-direction offsets in four postures in the five gait cycles in the figure, the offset in the lateral swing posture of $\theta_1 = 20^\circ$ is the smallest, indicating that the lateral swing posture is advantageous for the stability of the quadruped robot, its walking is more stable than walking in an upright posture, and the static stability of the robot is higher as the lateral swing angle increases.

When the robot's legs swing laterally outward to form a new leg posture, the robot's support area is relatively expanded, and the increments of the moment M_m that the body's center of mass acts on the flip axis increase with time. Therefore, the center of mass of the robot moves toward the center of the support area more easily than the original posture. At the same time, the vertical momentum of the body is relatively reduced, and the tilt of the body is correspondingly smaller, so the stability is higher.

5. Conclusions

A stable balance adjustment structure for the legs of a quadruped robot based on a bionic lateral swing posture is designed, and the leg kinematics model is established in this paper. The torque expression for tilting the quadruped robot is given by solving the hip joint momentum moment of the robot's swing phase. The obtained kinematic model was used to determine the relationship between the foot position and posture with the lateral swing angle. The relationship between the foot position and posture with the lateral swing angle is determined by using the obtained kinematic model, and the static stability conditions of the quadruped robot in the upright posture and the bionic lateral swing posture are given. The walking motion simulation and comparative analysis of the two postures of the robot were carried out based on Adams. The experimental simulation results show that the forward turning moment increases with the increase of the lateral swing angle during the process of switching the hind legs from the support phase to the swing phase, and the body's inclination decreases with the increase of the lateral swing angle, so that the bionic horizontal posture of the quadruped robot has higher static stability compared to the traditional upright posture. When the walking stability of the robot is insufficient, the tilting degree of the robot can be reduced by laterally swinging the legs outwards to realize the offline continuous walking of the robot. These research results provide a technical reference for the design and optimization of the offline continuous gait of the robot and the improvement of stability.

Data Availability

The data used to support the findings of this study are available from the corresponding author upon request.

Conflicts of Interest

The authors declare that there are no conflicts of interest regarding the publication of this paper.

Acknowledgments

This work was supported by the National Natural Science Foundation of China (No. 61650106) and Foundation of Guilin University of Technology (No. GLUTQD2013007).

References

[1] X. D. Li, H. W. Gao, J. Li et al., "Hierarchically planning static gait for quadruped robot walking on rough terrain," *Journal of Robotics*, vol. 2019, Article ID 3153195, 12 pages, 2019.

[2] D. Wojtkowiak, K. Talaśka, I. Malujda et al., "Modelling and static stability analyses of the hexa-quad bimorph walking robot," *MATEC Web of Conferences*, vol. 254, Article ID 02029, 2019.

[3] Y. Farid, V. Majd, A. Ehsani-Seresht et al., "Dynamic-free robust adaptive intelligent fault-tolerant controller design with prescribed performance for stable motion of quadruped robots," *Adaptive Behavior*, vol. 2019, Article ID 105971231989069, 2019.

[4] M. F. Chen, H. Chen, X. J. Wang et al., "Design and control of a novel single leg structure of electrically driven quadruped robot," *Mathematical Problems in Engineering*, vol. 2020, Article ID 3943867, 2020.

[5] T. Nemoto, R. E. Mohan, and T. D. Abbott, "Rolling locomotion control of a biologically inspired quadruped robot based on energy compensation," *Journal of Robotics*, vol. 2015, Article ID 649819, 10 pages, 2015.

[6] M. M. Gor, P. M. Pathak, A. K. Samantaray, J.-M. Yang, and S. W. Kwak, "Fault accommodation in compliant quadruped robot through a moving appendage mechanism," *Mechanism and Machine Theory*, vol. 121, pp. 228–244, 2018.

[7] W. He, C. Q. Xue, X. B. Yu et al., "Admittance-based controller design for physical human–robot interaction in the constrained task space," *IEEE Transactions on Automation Science and Engineering*, In press, 2020.

[8] W. He, H. J. Gao, C. Zhou et al., "Reinforcement learning control of a flexible two-link manipulator: an experimental investigation," *IEEE Transactions on Systems, Man, and Cybernetics: Systems*, In press, 2020.

[9] Y. Farid, V. J. Majd, A. Ehsani-Seresht et al., "Fractional-order active fault-tolerant force-position controller design for the legged robots using saturated actuator with unknown bias and gain degradation," *Mechanical Systems and Signal Processing*, vol. 104, pp. 465–486, 2017.

[10] H. Park, B. Kwak, and J. Bae, "Inverse kinematics analysis and COG trajectory planning algorithms for stable walking of a quadruped robot with redundant DOFs," *Journal of Bionic Engineering*, vol. 15, no. 4, pp. 610–622, 2018.

[11] W. T. Zhao and Z. Z. Liu, "The foot workspace analysis of quadruped bio–robot," *Machine Design and Manufacturing Engineering*, vol. 40, no. 13, pp. 19–22, 2011.

[12] X. Q. Lv and M. Zhao, "Application of improved BQGA in robot kinematics inverse solution," *Journal of Robotics*, vol. 2019, Article ID 1659180, 7 pages, 2019.

[13] L. Bai, L. H. Ma, Z. F. Dong et al., "Kinematics, dynamics, and optimal control of pneumatic hexapod robot," *Mathematical Problems in Engineering*, vol. 2017, pp. 1–16, Article ID 6841972, 2017.

[14] C. Zhang and J. Dai, "Trot gait with twisting trunk of a metamorphic quadruped robot," *Journal of Bionic Engineering*, vol. 15, no. 6, pp. 971–981, 2018.

[15] J. X. Shen, H. G. Cui, K. Feng et al., "Parameter identification and control algorithm of electrohydraulic servo system for robotic excavator based on improved hammerstein model," *Mathematical Problems in Engineering*, vol. 2020, Article ID 9216019, 9 pages, 2020.

[16] T. Zhang, X. K. Yue, B. Dou et al., "Online one-step parameter identification method for a space robot with initial momentum in postcapture," *Journal of Aerospace Engineering*, vol. 33, no. 4, Article ID 04020029, 2020.

[17] Y. N. Zhang, X. S. Wang, Y. H. Xin et al., "Quadruped robot leg optimization based on a multi-objective genetic algorithm," *Mechanics*, vol. 23, no. 6, pp. 881–890, 2018.

[18] X. H. Tian, F. Gao, C. K. Qi et al., "Reaction forces identification of a quadruped robot with parallel-serial leg structure," *Mechanical Engineering Science*, vol. 229, no. 15, pp. 2774–2787, 2017.